Palaeogeography, Palaeoclimatology, Palaeoecology 313-314 (2012) 181–188

Contents lists available at SciVerse ScienceDirect

Palaeogeography, Palaeoclimatology, Palaeoecology

journal homepage: www.elsevier.com/locate/palaeo

Cessation of a productive coastal upwelling system in the Panthalassic Ocean at the Permian–Triassic Boundary

Shane D. Schoepfer [a,*], Charles M. Henderson [b], Geoffrey H. Garrison [a], Peter D. Ward [a]

[a] University of Washington
[b] University of Calgary

ARTICLE INFO

Article history:
Received 26 March 2011
Received in revised form 16 October 2011
Accepted 30 October 2011
Available online 6 November 2011

Keywords:
Permian
Extinction
Panthalassic
Conodonts
Nitrogen
Anoxia

ABSTRACT

While the end-Permian extinction in the marine realm is well known from the Tethys Ocean, it remains little studied in the vast Panthalassic Ocean. Opal Creek, Alberta, Canada is a biostratigraphically continuous Permian–Triassic Boundary (PTB) section that is interpreted to have been deposited in a deep outer shelf setting along the Panthalassic western margin of Pangaea. Significant organic carbon and nitrogen isotope excursions precede the extinction of the dominant Late Permian benthic organisms (siliceous sponges). Geochemical comparison with underlying Guadalupian age rocks and analysis of the conodont fauna suggest that the latest Permian at Opal Creek records the shutdown of a productive cold-water upwelling ecosystem with a mid-water column oxygen minimum followed by the transition to a warm and less vigorously circulating system with a bottom-water oxygen minimum. The transition from a low-diversity, cold-water conodont fauna in the Middle Permian to a more diverse latest Permian fauna containing equatorial species coincides with a transition from elevated $\delta^{15}N$ values characteristic of coastal zones with denitrification in a mid-water oxygen minimum to more normal marine values. A spike in the $\delta^{13}C$ of organic carbon following a latest Permian marine transgression along western Pangaea is here attributed to transient increased productivity in the photic zone preceding the main extinction, likely related to the synergistic effects of warming, increased nutrient runoff, and residual upwelling. This is followed by an equilibration to lower $\delta^{13}C_{org}$ values characteristic of a lower productivity regime in the Early Triassic.

1. Introduction

The Panthalassic Ocean, covering some 70% of the globe, was the largest surficial feature of the Permian and Triassic world, and had the potential to exercise fundamental control of global biogeochemistry. Unfortunately, the sparsity of preserved sedimentary records has made Panthalassic ecology difficult to study. Here we examine outer shelf marine sediments from the eastern Panthalassic Ocean to determine the ecosystem's response to environmental perturbations associated with the Permian–Triassic extinction, the greatest biodiversity crisis of the Phanerozoic, which fundamentally and irrevocably altered marine ecosystems for the entirety of subsequent geologic time (Raup and Sepokoski, 1982).

Many potential mechanisms have been proposed for the Permian–Triassic mass extinction, ranging from extraterrestrial impact (Becker et al., 2001) to rapid warming of climate (Kidder and Worsley, 2004; Kump et al., 2005). However, the exact mechanism of extinction remains poorly understood, in part because the majority of the available data is drawn from a limited region of the Permian world surrounding the Tethys Ocean (e.g. Baud et al., 1989; Jin et al., 2000; Brookfield et al., 2003.), with the exception of the mid-Panthalassic oceanic sediments exposed in Japan (Isozaki, 1994, 1997; Algeo et al., 2010a, 2010b).

Among the Late Permian through Early Triassic environmental disruptions that may have been causally related to the extinction are changes in crustal weathering patterns (Kidder and Worsley, 2003), changes in paleosols in non-marine sections (Retallack et al., 2003), aridification, vegetation loss, and fluvial drainage alteration (Ward et al., 2000), greenhouse conditions and warming of the global ocean due to massive volcanic eruptions and increased atmospheric CO_2, as well as possible methane clathrate releases (Benton and Twitchett, 2003, Winguth et al. 2002). Warm temperatures are determined by warm climate flora at polar latitudes (Taylor et al., 2000), as well as the global demise of high latitude, cool-water, siliceous sponges (Henderson, 1997; Beauchamp and Baud, 2002), and a breakdown of temperature-based conodont provincialism (Mei and Henderson, 2001). There is also growing evidence that between the Middle Permian and Early Jurassic the oxygen content of Earth's atmosphere may have varied markedly with important biological consequences (Wignall and Hallam, 1992, 1993; Wignall and Twitchett, 1996; Berner and Kothavala, 2001; Berner, 2002; Retallack et al., 2003; Huey and Ward, 2005).

* Corresponding author at: Department of Earth and Space Sciences, University of Washington, Johnson Hall Rm-070, Box 351310, 4000 15th Avenue NE.
E-mail address: shanedms@uw.edu (S.D. Schoepfer).

0031-0182/$ – see front matter © 2011 Elsevier B.V. All rights reserved.
doi:10.1016/j.palaeo.2011.10.019

Dramatic changes in inorganic and organic $\delta^{13}C$ records characterize Permian/Triassic Boundary (PTB) geochemical records in the available rock record (Retallack et al., 2003; Payne et al., 2004; Peter et al. 2005), with a negative excursion characterizing the latest Permian in Tethyan sections (Korte and Kozur, 2010; Luo et al., 2011). Negative shifts have been explained by addition of ^{13}C-depleted CO_2 to the global atmosphere–ocean reservoir by catastrophic methane release and oxidation (Retallack et al., 2003), exposure and oxidation of buried organic matter (Berner, 2002), anoxic ocean overturn (Knoll et al., 1996), and CO_2 release during massive volcanism (Erwin et al., 2002; White, 2002). Positive shifts in the organic $\delta^{13}C$ of marine sediments, which have been observed in other Panthalassic deep water sections (Isozaki, 2009) have proven more difficult to explain, potentially reflecting both changes in the productivity and composition of marine planktonic communities (O'Leary, 1981, 1988), and variation in the degree to which various organic components (such as proteins) are preferentially degraded in a stratified versus pervasively anoxic ocean (Isozaki, 2009). As productivity and associated biological oxygen demand may have fueled Permian marine anoxia, it is important to understand the interplay between Panthalassic biology and oxygen availability.

Here we present the results of a carbon and nitrogen isotope study from a section in Southwest Alberta–Opal Creek. Sediments that comprise these strata were deposited in an outer shelf setting in the Panthalassic Ocean, on the downwarped western margin of the North American plate (Henderson, 1989; Richards, 1989) at approximately 30° North paleolatitude. This site has a complete conodont zonation from the uppermost Permian across the PTB in an area far removed from the Tethyan basin. The site is the southernmost of a series of Upper Permian–Lower Triassic sections running north into the Arctic. This environmental record from off the northwest shores of Pangaea provides augmentation to the numerous Tethyan and mid-Panthalassic studies and improves our understanding of environmental changes across the world's largest ocean basin. This site contains a well-preserved boundary interval deposited in a deep-water facies, with sufficient biostratigraphic control to allow global correlation (Henderson et al., 1994; Henderson, 1997).

1.1. Geologic setting and biostratigraphy

The Opal Creek Permian–Triassic boundary section is located in southwest Alberta, along the southern bank of Opal Creek in the Kananaskis Valley in the foothills of the Canadian Rockies (Fig. 1). The Ranger Canyon and Fantasque formations, consisting of spiculitic chert grading into carbonate and silica cemented immature sandstone and phosphatic siltstones, (Fig. 3) range from southeastern British Columbia to the southern Mackenzie Fold Belt in northern Canada (Henderson, 1989). These units were deposited on a deep water outer shelf or slope as determined by the predominance of sponge spicules, the abundance of phosphatic material, and the absence of shallow water sedimentary structures (Henderson, 1997). At Opal Creek, the Ranger Canyon Formation is only 235 cm thick and includes the conodonts *Mesogondolella bitteri* and at the top *M. rosenkrantzi*; indicating a Capitanian age (Mei and Henderson, 2001). The presence of *M. rosenkrantzi* may indicate an early Wuchiapingian or latest Capitanian age given the overlap with *M. bitteri* (Mei and Henderson, 2001). Middle and Late Permian species of *Mesogondolella* are typical of cool-water environments as inferred by their strong boreal provincialism (Mei and Henderson, 2001) at that time. The most common fossils in the Ranger Canyon Formation chert are large monaxon siliceous sponges spicules (up to 6 cm long), of the class Demospongea. Elsewhere, the presence of these "silica factories" has been used to infer nutrient-rich, cold marine waters with active oceanic circulation (Beauchamp and Baud, 2002).

Unconformably overlying the Ranger Canyon Formation is the Phroso Siltstone Member of the Sulphur Mountain Formation, equivalent to the Grayling Formation in northeastern British Columbia (Wignall and Newton, 2003), which is composed of silty shale with minor dolomite, as well as abundant pyrite, which is especially concentrated in a cm-think bed located 10.5 cm above the unconformity.

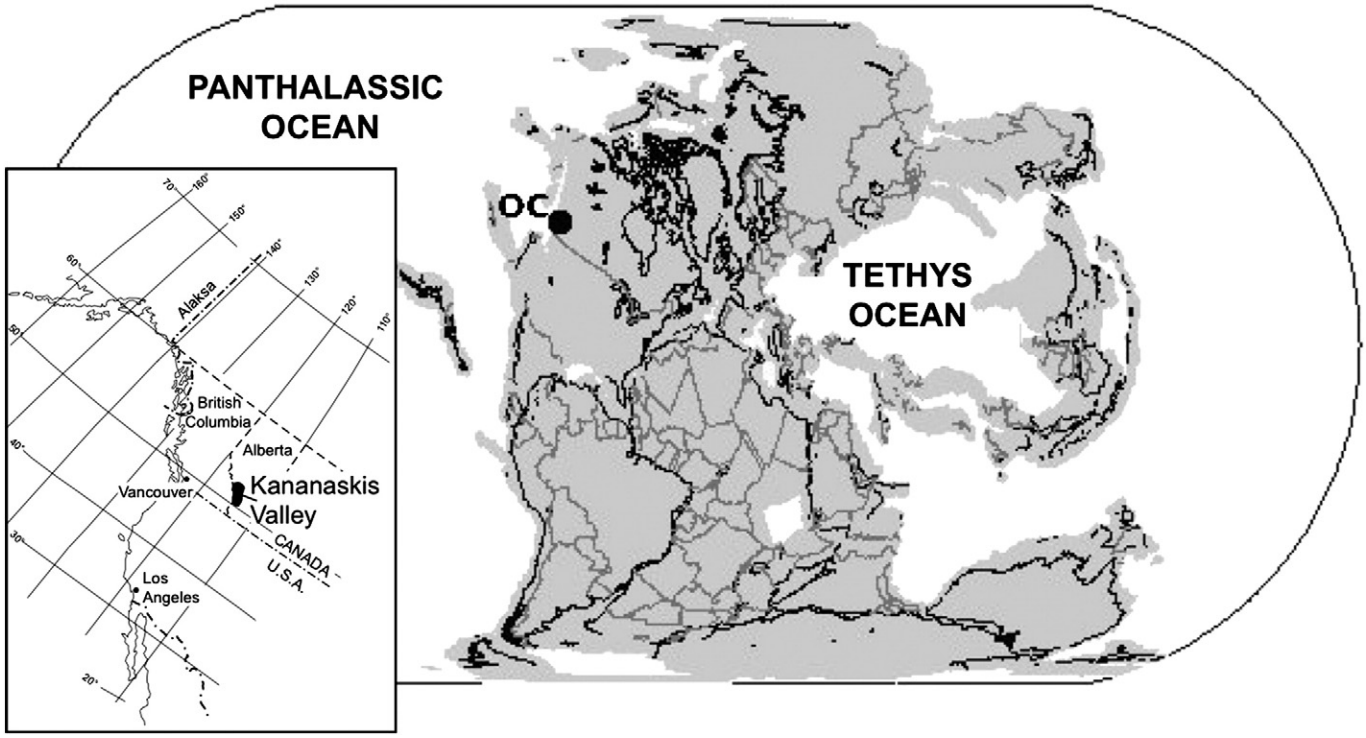

Fig. 1. Paleomap showing the position of the continents and oceans in the latest Permian. OC = location of Opal Creek section. Map software from PaleoDB, copyright Alroy 2010. Inset displays the modern location of the Kananaskis Valley in Alberta.

Like the Ranger Canyon, the lower most Sulphur Mountain Formation also has abundant siliceous monaxon sponge spicules to 2 cm in length and triaxon siliceous hyalosponge spicules. These disappear abruptly at 0.4 m above the base, which coincides with the sudden influx of new Late Permian conodont species belonging to the genus *Clarkina,* likely representing the main end-Permian extinction. Above this boundary, the Sulphur Mountain Formation is composed of black to dark grey, pyritic, thin-bedded shale and siltstone. There is a dearth of benthic biota or bioturbation, suggesting suboxic to anoxic bottom waters during deposition (Fig. 2) (Gibson, 1969, 1974; Gibson and Barclay, 1989; Henderson, 1997).

The temporal extent of the regional unconformity can be approximated using conodont biostratigraphy from carbonate lenses within the Ranger Canyon Formation and from slightly calcareous silty shale of the Sulphur Mountain Formation. The oldest rocks of the Sulphur Mountain Formation include *Mesogondolella sheni* and presumed reworked specimens of *M. bitteri* and *M. rosenkrantzi*. *M. sheni* appears to be a good index for the cool-water Changhsingian (Mei and Henderson, 2001) and is widely distributed from Selong, Tibet (Mei, 1996) to the Sverdrup Basin in the Canadian Arctic (Beauchamp et al., 2009). The presence of *M. sheni* from the basal transgressive systems tract (TST) of the Sulphur Mountain Formation indicates a Changhsingian age, but the exact relationships between these specimens and the type material from Selong, Tibet (Mei, 1996; Shen et al., 2006) still need to be established. The duration of the unconformity separating the Ranger Canyon and Sulphur Mountain formations includes all or most of the Wuchiapingian and part or most of the Changhsingian and is therefore on the order of 5 to 7 million years (Shen et al., 2010).

Four conodont biozones comprise the studied portion of the Sulphur Mountain Formation at Opal Creek, including in ascending order: 1) *M. sheni*, 2) *C. hauschkei – C. meishanensis*, 3) *Hindeodus parvus – C. taylorae*, and 4) *C. taylorae – C. cf. carinata* Zones (Fig. 3), with the local first occurence of *H. parvus* in association with the first occurence of C. taylorae at 150 cm above the unconformity indicating the biostratigraphic Permian–Triassic Boundary.

2. Materials and methods

Samples 0.5 kg – 3 kg in mass were collected at meter scale throughout the section for conodont biostratigraphy. Additionally, samples 3–10 g in mass were collected at meter to sub-centimeter scale in the lowermost strata surrounding the PTB, for isotopic analysis Sedimentary organic $\delta^{13}C_{org}$ and $\delta^{15}N$ were analyzed via elemental analyzer-continuous-flow isotope ratio mass spectrometry (EA-CFIRMS) at the ISOLAB stable isotope laboratory at the University of Washington. Samples were chosen to avoid cracks and visible surface alteration and weathering and sonicated in methanol and deionized water. Samples were then powdered and acidified with an excess of 10% HCl and kept at 40 °C for at least 12 h to remove inorganic carbonate material. Samples were then triple rinsed with ultra pure (>18 MΩ) deionized water and oven dried at 40 °C. Analyses were made with a Costech ECS 4010 Elemental Analyzer coupled to a ThermoFinnigan MAT253 mass spectrometer via a ThermoFinnigan CONFLO III gas interface.

Carbon and oxygen isotopes ($\delta^{13}C_{carb}$ and $\delta^{18}O_{carb}$) of the carbonate fraction of the cherts and siltstones were measured by IRMS on a Micromass Isoprime dual inlet mass spectrometer. Samples were introduced via a Micromass carbonate autosampler system. Samples were held in evacuated 5 ml vacutainers with proprietary CO_2-impermeable seals and acidified with 103% (dehydrated) phosphoric acid at 90 °C for 10 min; the evolved CO_2 was cryogenically stripped of water vapor prior to being introduced to the mass spectrometer.

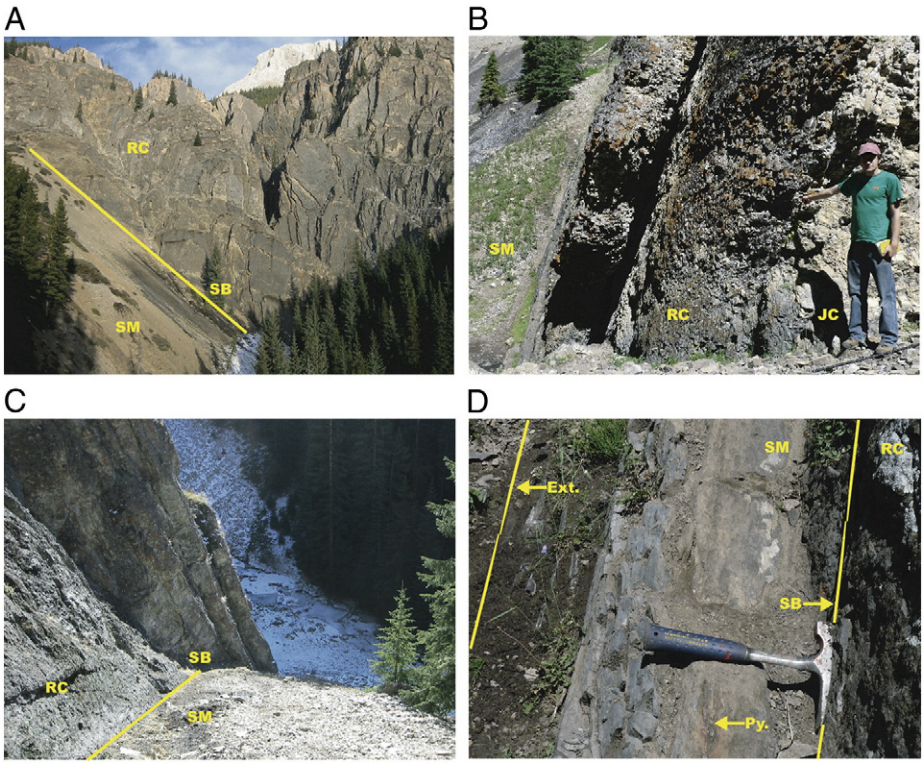

Fig. 2. Photograph of outcrop at Opal Creek. A: Facing outcrop from trail. Beds dip nearly vertically, cliff forming unit is the Ranger Canyon Formation, with the face representing the unconformable upper contact. The Sulfur Mountain siltstones form most of the slope in the foreground. B: Cross sectional view of Ranger Canyon formation, author pointing to lower contact with underlying Johnston Canyon dolostones. Ranger Canyon unit is approximately 2 m. thick. C: View along cliff face showing contact between resistant, silicified Ranger Canyon material and fissile Sulphur Mountain siltsones. D: Close up of latest Permian deposits following the unconformity at Opal Creek. Rock hammer for scale. JC = Johnston Canyon Formation, RC = Ranger Canyon Formation, SM = Sulphur Mountain Formation, SB = Unconformable sequence boundary, Py. = Pyrite bed, Ext. = main extinction horizon.

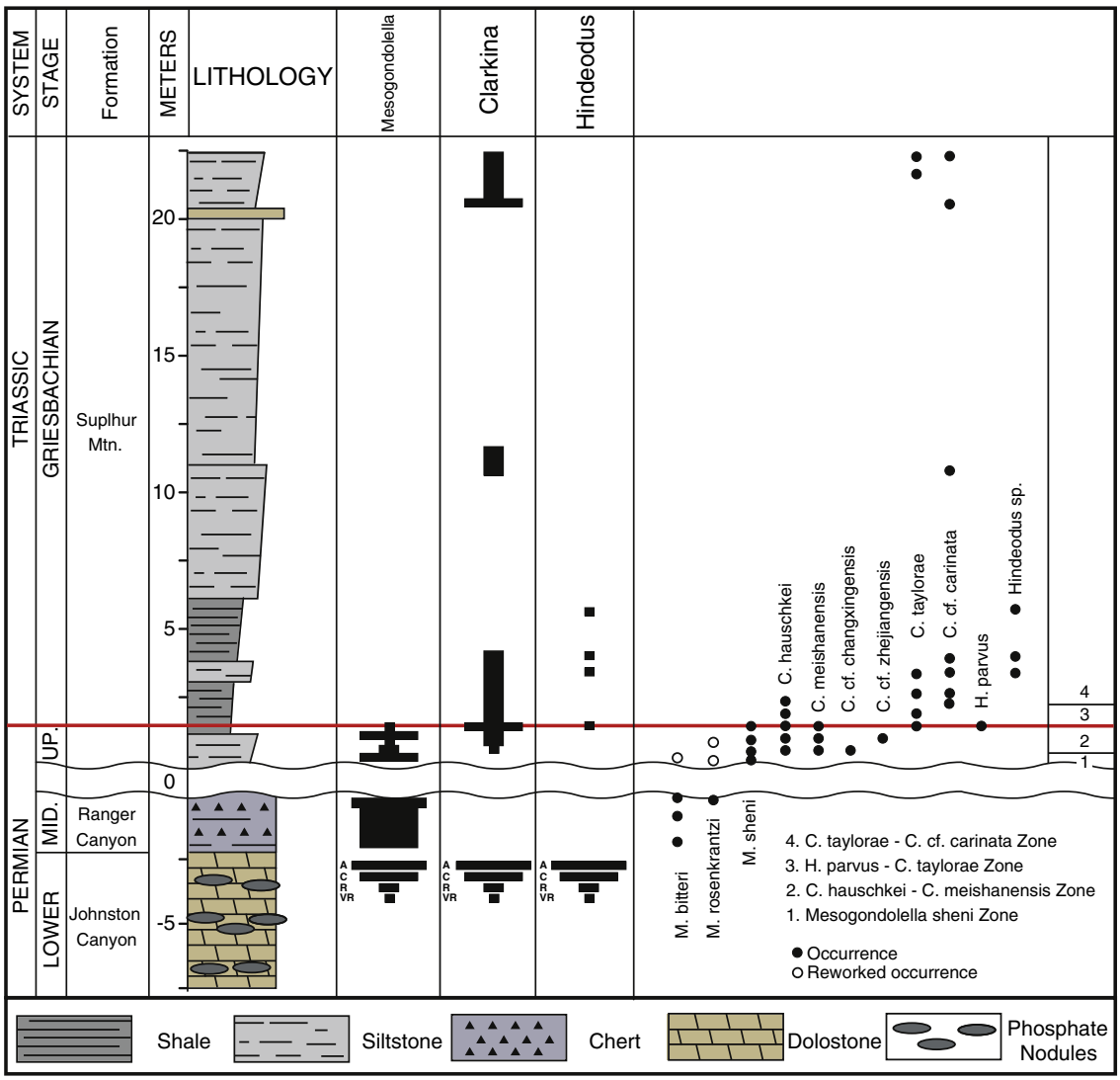

Fig. 3. Stratigraphic column of the Opal Creek section, showing conodont occurrences and zonation, as well as the abundances of three conodont genera. A = Abundant (>20/kg), C = common (10–20/kg), R = Rare (5–10/kg), VR = Very Rare (1–5/kg). Only P1 conodont elements were counted, samples were each approximately 2–3 kg of rock.

All stable isotope ratios are reported in standard delta (δ) notation indicating the per mil (‰) difference from a standard with an accepted value such that:

$$\delta = \left(R_{sample}/R_{std.} - 1\right) \cdot 1000$$

where R equals $^{15}N/^{14}N$ for nitrogen and $^{13}C/^{12}C$ for carbon. The standard for nitrogen is air; the standard for carbon and oxygen is Vienna PeeDee Belemnite (VPDB).

The standard deviation (σ) of sample replicates was 0.15‰ for $\delta^{13}C_{org}$ ($n = 36$), 0.26‰ for $\delta^{15}N$ ($n = 57$), 0.10‰ for $\delta^{13}C_{carb}$ ($n = 50$), and 0.25‰ for $\delta^{18}O_{carb}$ ($n = 50$). Analytical precision based on routine analyses of internal laboratory reference materials was 0.15‰ for $\delta^{13}C_{org}$, 0.10‰ for $d^{15}N$, and 0.32‰ for $\delta^{13}C_{carb}$ and $\delta^{18}O_{carb}$. Many samples contain low levels of nitrogen, to avoid error, we here report only samples with an integrated peak area of >12 mV at mass 28.

Samples generally contain high Total Organic Carbon, ranging from 0.52 to 3.37% and generally increasing upward throughout the section (Fig. 5), and thus organic carbon isotopes are unlikely to reflect contamination by hydrocarbon fluids. The Conodont Alteration Index (CAI) for conodont elements at Opal Creek is 2.5, suggesting low to moderate thermal alteration of the sediments.

Chemical composition of the samples was measured by the ALS Chemex company of Vancouver, BC, using Inductively Coupled Plasma Atomic Emission Spectroscopy (ICP-AES). A 0.25 g sample was digested in hydrochloric, nitric, perchloric and hydrofluoric acids. The residue was suspended in dilute HCl and analyzed for element composition by ICP-AES, with sub-ppm lower detection limits for most elements. In order to determine the nature of carbonate minerals in the section, eight thin sections were prepared and examined with a petrographic microscope.

3. Results

3.1. Carbonates

The $\delta^{18}O$ of the carbonate fraction was measured at 151 points in the Middle Permian Ranger Canyon Formation and across the PTB in the first 22 m of the Sulphur Mountain Formation. These display a wide range of variation, with $\delta^{18}O$ from −10.62‰ to −2.68‰. The $\delta^{13}C$ of inorganic carbonate was measured at 152 points, and ranges from −9.22‰ to −1.20‰. Thin-section petrography of Opal Creek sediments revealed carbonates present as microcrystalline cements, dolomite rhombs, and reworked calcite grains. As multiple generations of carbonate are present, and isotope values indicate almost

certain diagenetic alteration, carbonate isotopes are not assumed to reflect depositional conditions and will not be considered further. However, the lack of correlation between organic and inorganic carbon isotopes ($R^2 = 0.031$, Fig. 4) suggests that the organic carbon signal is not a function of diagenetic alteration.

3.2. Organic carbon

The $\delta^{13}C$ of organic carbon was measured at 191 points throughout the section (Fig. 5). Organic carbon isotopes showed a stable equilibrium at $-29.36 \pm 0.41‰$ ($n = 12$) throughout the Ranger Canyon Formation. The Sulphur Mountain sediments immediately overlying the unconformity have similar values. However, there is a dramatic spike to values as high as $-25.68‰$ in the section's most pyritic interval at 10.5 cm After the excursion, organic carbon isotopes settle to a steady equilibrium with a mean $\delta^{13}C$ of $-31.21 \pm 0.48‰$ ($n = 169$).

3.3. Nitrogen

Nitrogen isotopes were measured at 58 points across the PTB and in the underlying strata (Fig. 5). Nitrogen isotope values in the Ranger Canyon Formation are generally quite high, with a mean value of $8.13 \pm 0.97‰$, ($n = 9$). Nitrogen values peak in the lowermost Sulphur Mountain, reaching values as high as 10.14‰ in the 10.5 cm above the unconformity. The most pyritic interval of the section, at 10.5 cm, corresponds to a rapid drop off in $\delta^{15}N$ to values averaging $2.92 \pm 0.41‰$ for the laminated siltstones ($n = 42$), a more typical value for marine sedimentary organic matter.

3.4. Aluminum content

The presence of reworked conodonts around the unconformity indicates that some mixing of sediments has occurred. In order to assess the degree to which reworking or biological mixing of sediments can explain the resemblance of nitrogen isotopes in the lowermost Sulphur Mountain Formation to the middle Permian Ranger Canyon Formation, we measured the aluminum content of samples at 25 points throughout the section. Aluminum varies markedly between the Ranger Canyon Formation and Sulphur Mountain Formation lithologies, and is relatively unaffected by biochemical processes in the ocean (Tribovillard et al., 2006), which makes it useful as a measure of the degree to which material has been physically mixed across the contact. Exclusive of the points immediately above and below the unconformity, the Ranger Canyon Formation has an average aluminum content of 0.53% (s = 0.25%), whereas the Sulphur Mountain Formation has a much higher average of 7.08% (s = 0.86%). The samples immediately surrounding the unconformity had intermediate values, with a simple mixing model suggesting an approximately 13% contribution of Sulphur Mountain material to the uppermost measured Ranger Canyon sample, 4 cm below the unconformity, and a 22% contribution of Ranger Canyon material to the lowermost measured Sulphur Mountain sample, 10.5 cm above the unconformity.

Assuming similar nitrogen content, this is sufficient to explain the high nitrogen value measured in the pyrite bed at 10.5 cm However, it is inconsistent with the maximum $\delta^{15}N$ values being measured just above the unconformity, as well as the lack of an apparent Sulphur Mountain Formation contribution to the uppermost Ranger Canyon Formation . Furthermore, the discrete peak in organic carbon isotopes at 10.5 cm as well as the presence of an uninterrupted centimeter thick pyrite bed suggests that mixing was not the primary control of the geochemistry of this interval.

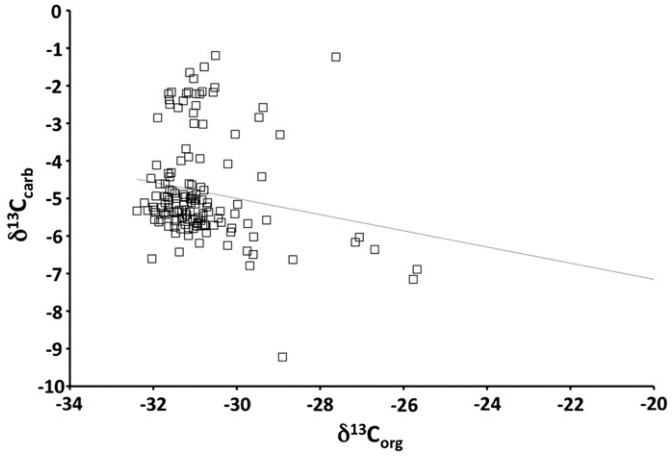

Fig. 4. Crossplot of organic and inorganic carbon isotopes with best-fit regression. $R^2 = .031$. Lack of correlation suggests organic carbon isotopes have not been affected by diagenesis.

4. Discussion

Here we interpret the disappearance of siliceous sponge spicules, 40 cm above the beginning of the Sulphur Mountain Formation transgressive sequence, as representing the principal Permian–Triassic marine extinction event. The disappearance of chert units at higher latitudes along the latest Permian Panthalassic margin of Pangaea has been previously described by Beauchamp and Baud (2002) who suggest that siliceous sponges thrived in cold bottom water, which would contain higher levels of dissolved oxygen and suppress competition from carbonate producers. Our nitrogen and organic carbon isotope data support the hypothesis that a shutdown of cold-water upwelling and the corresponding high organic productivity occurred along the western margin of Pangaea in the latest Permian, leading to the demise of the sponges. Such a breakdown of longstanding circulation patterns and the consequent decrease in deepwater oxygen concentrations may be attributable to warming of the latest Permian oceans and consequently the cessation of thermally-driven ocean circulation and warming of the deep ocean (Kiehl and Shields, 2005).

As nitrate utilization in the surface ocean is typically complete at low latitudes (Sigman and Boyle, 2000), the available nitrate pool in the original Middle Permian water column overlying Ranger Canyon sediments may have had a $\delta^{15}N$ of 7–10‰. This enrichment likely reflects the presence of a mid-water column anoxic zone, where denitrification was taking place (Algeo et al., 2008). This anaerobic process, whereby nitrate is reduced to N_2 gas, imparts a large fractionation effect ($\varepsilon = -20‰$, Brandes and Devol, 2002) and strongly enriches the remaining nitrate pool. Such mid-water anoxic zones are known from many modern regions of the ocean, such as the Peru Margin and Arabian Sea, where upwelling nutrients fuel rapid export of organic matter from the photic zone (Brandes and Devol, 2002). Such regions often have sedimentary $\delta^{15}N$ values in the 7–10‰ ranges (Algeo et al., 2008)

As a result of these processes, the intensity of the coastal upwelling system can be inferred from the $\delta^{15}N$ of organic matter in the underlying sediments. The persistence of strong upwelling into the latest Permian can be seen in the enriched nitrogen isotope values of the lowermost Phroso Siltstone, from samples above the unconformity surface. We propose that the subsequent shift to a sedimentary $\delta^{15}N$ of 2–3 represents the final collapse of the mid-water denitrification zone and the productive cold-water upwelling system that had persisted along the western margin of Pangaea since the Artinskian (Beauchamp and Baud, 2002). This would correspond to a transition to lower productivity conditions, and an increased reliance on nitrogen fixed directly from the atmosphere ($\delta^{15}N = 0$). Under such conditions of slowing circulation, the water column likely transitioned from having a mid-water oxygen minimum to a bottom-water oxygen minimum, which would contribute to the general increase in organic carbon content (through increased preservation) and conspicuous lack of bioturbation in the earliest Triassic.

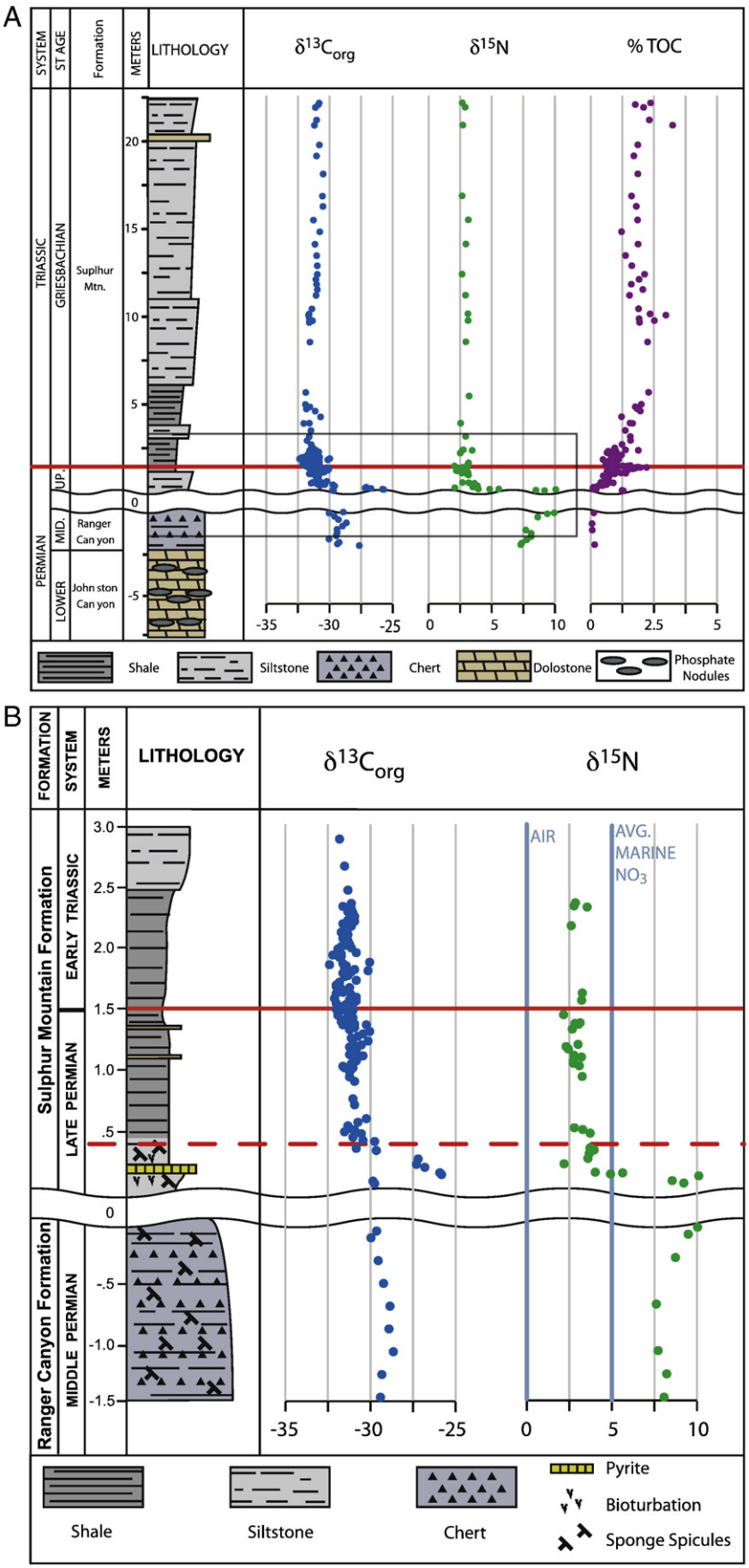

Fig. 5. A: Stratigraphic column of the Opal Creek section showing organic carbon isotopes (VPDB) and nitrogen isotopes (AIR), as well as % Total Organic Carbon (TOC). Highlighted area is expanded in B: Expanded stratigraphic column of shaded area around Permian Triassic Boundary. Dashed red line indicates main extinction horizon, solid red line indicates biostratigraphic PTB Vertical lines on nitrogen graph show the isotopic values of atmospheric N_2 (AIR) and an average value of modern marine nitrate (NO_3^-).

While positive organic carbon isotope excursions may be attributed to the rapid burial of light organic carbon biomass following a mass die-off, the major $\delta^{13}C_{org}$ excursion at Opal Creek precedes the main extinction event at 40 cm. Changes in the total carbon pool, such as an addition of carbon to the atmosphere through volcanism or methane degassing are expected to decrease $\delta^{13}C$ (Korte et al., 2010; Luo et al., 2011).

The pre-extinction positive spike in $\delta^{13}C_{org}$ at Opal Creek may represent a decrease in photosynthetic fractionation, possibly indicating a pulse of high productivity, in which organisms were competing to uptake dissolved carbon (a situation described as carboxylation-limitation), (O'Leary, 1988). Such decreases in photosynthetic fractionation have also been interpreted as cyanobacteria using the β-carboxylation pathway (Kashiyama et al., 2008), and cyanobacteria may have become predominant in an increasingly nitrogen limited environment (Luo et al., 2011). Alternatively, this may represent the increasing contribution of anoxygenic photosynthsizers, which show a smaller carbon fractionation effect than oxygenic photosynthesizers (O'Leary, 1981) and may be associated with the expansion of photic zone euxinia in the latest Permian world as indicated by the presence of a pyrite interval (Grice et al., 2005; Grasby and Beauchamp, 2009). No combination of these explanations is consistent with a collapse of marine productivity prior to the main extinction event. Following this interpretation, the return to a lower equilibrium $\delta\ ^{13}C_{org}$ in the post-extinction Sulphur Mountain Formation likely represents a lower productivity regime in an increasingly nutrient limited environment, though the addition of light volcanic or methanogenic carbon to the dissolved carbon pool may have also played a role.

It is noteworthy that these isotope transitions correspond to the beginning of significant ecological diversity in the conodont fauna, with several species of the genus *Clarkina* appearing in significant numbers alongside *Mesogondolella*. The Ranger Canyon ecosystem was dominated by high abundances of a single species, *Mesogondolella bitteri*, which is replaced by abundant *M. sheni* in the lowermost Sulphur Mountain. High-abundance, low-diversity ecosystems in the fossil record have been interpreted to represent eutrophic environments (Brasier, 1995), which favor organisms that can rapidly exploit the available resources, and all of these conodonts displayed strong cold-water provincialism. The transition to a more diverse conodont fauna, including the previously equatorial genus *Clarkina*, corresponds temporally to the drop in sedimentary $\delta^{15}N$, providing further support for the collapse of a eutrophic coastal upwelling environment (Fig. 3), with the loss of cold upwelling surface water removing a temperature barrier to migration (Mei and Henderson, 2001).

The essentially coterminous peaks in $\delta^{13}C_{org}$ and $\delta^{15}N$ suggest that the decrease in productivity associated with the termination of upwelling was not a monotonic trend. This interval may represent a transient period of increased algal productivity at Opal Creek, relative to the subsequent Sulphur Mountain Formation. This increase may have been due to the synergistic effects of the residual deepwater upwelling, with its high nutrient content, which may have been further aggravated by additional nutrient runoff from the Pangaean continent (Ward et al., 2000; Wignall and Newton, 2003; Algeo et al., 2010b) and the sudden warming of the Permian sea surface. When warming advanced to the point of stopping the upwelling system, productivity returned to lower levels. Such a spike in sinking organic flux would have created extreme biological oxygen demand and may have driven high levels of biological sulfate reduction, contributing to end-Permian euxinia (Grice et al., 2005; Kump et al., 2005; Meyer and Kump, 2008; Grasby and Beauchamp, 2009), with photosynthetic sulfur bacteria possibly surviving in the photic zone (Hays et al., 2007).

Such an expansion of anoxic waters into the shallow photic zone, whether driven by increased productivity or not, may also have contributed to a positive organic carbon isotope excursion by creating more homogenous redox conditions throughout the water column. By weakening vertical redox gradients, the preferential degradation of certain organic components (mainly proteins) in oxic waters and its associated isotope fractionation would have been reduced. This has been observed by Isozaki (2009) in several deep water Panthalassic sections accreted onto Japan. As the opposite (a negative $\delta^{13}C_{org}$ excursion) was seen in shallow-water atoll carbonates, the positive excursion at Opal Creek would support the conclusion that the section was deposited below the chemocline, even prior to the PTB crisis interval.

It is unclear if the termination of upwelling represented the return to "normal" marine conditions or to the stratified ocean hypothesized for the Permian–Triassic boundary (Isozaki, 1994; Wignall and Newton, 2003). Stratification of the entire Panthalassic Ocean has proven difficult to sustain in models (Hotinski et al., 2001), and such an extreme condition would be likely to leave evidence in the stable isotope data. Trace metals from Panthalassic sections spanning the PTB have indicated suboxic rather than fully euxinic bottom waters (Algeo et al., 2010a).

5. Conclusions

Despite the Panthalassic Ocean's potentially dominant role in Permian biogeochemical cycling, there has been little direct evidence for biogeochemical changes leading up to the end-Permian extinction. While a slowing down or rearrangement of ocean circulation in the latest Permian has been previously proposed, here we present isotopic evidence for the cessation of coastal upwelling along western Pangaea.

Latest Permian deposits at Opal Creek display distinctive enrichments in ^{15}N and $^{13}C_{org}$, suggesting a period of elevated productivity and anoxia before the final termination of the western Panthalassic upwelling zone, the loss of benthic siliceous sponges, and the Permian/Triassic extinction. This productivity spike may have been due to the synergistic effects of nutrient upwelling and rapid warming and may have contributed to photic zone euxinia by increasing biological oxygen demand.

Supplementary materials related to this article can be found online at doi:10.1016/j.palaeo.2011.10.019.

Acknowledgments

The authors would like to acknowledge the generous support provided by The United States National Science Foundation (NSF) and NASA Astrobiology Institute (NAI) University of Washington node as well as the Natural Sciences and Engineering Research Council (NSERC) of Canada, and the University of Washington Earth and Space Sciences Department. Our special thanks as well to the staff of the University of Washington IsoLab facility for their extensive help with our isotopic analyses, and to our reviewers for their helpful feedback in preparing this manuscript for publication.

References

Algeo, T., Rowe, H., Hower, J.C., Schwark, L., Herrmann, A., Heckel, P., 2008. Changes in ocean denitrification during Late Carboniferous glacial-interglacial cycles. Nature Geoscience 1, 709–714. doi:10.1038/ngeo307.

Algeo, T.J., Hinnov, L., Moser, J., Maynard, J.B., Elswick, E., Kuwahara, K., Sano, H., 2010a. Changes in productivity and redox conditions in the Panthalassic Ocean during the latest Permian. Geology 38, 187–190. doi:10.1130/G30483.1.

Algeo, T.J., Kuwahara, K., Sano, H., Bates, S., Lyons, T., Elswick, E., Hinnov, L., Ellwood, B., Moser, J., Maynard, J.B., 2010b. Spatial variation in sediment fluxes, redox conditions, and productivity in the Permian–Triassic Panthalassic Ocean. Palaeogeography. doi:10.1016/j.palaeo.2010.07.007.

Baud, A., Magaritz, M., Holser, W.T., 1989. Permian–Triassic of the Tethys: carbon isotope studies. Geologische Rundschau 78, 649–677.

Beauchamp, B., Baud, A., 2002. Growth and demise of Permian biogenic chert along northwest Pangea: evidence for end-Permian collapse of thermohaline circulation. Palaeogeography, Palaeoclimatology, Palaeoecology 184, 37–63.

Beauchamp, B., Henderson, C.M., Grasby, S.E., Gates, L.T., Beatty, T.W., Utting, J., James, N.P., 2009. Late Permian sedimentation in the Sverdrup Basin, Canadian Arctic: the Lindström and Black Stripe Formations. Bulletin of Canadian Petroleum Geology 57, 167–191.

Becker, L., Poreda, R.J., Hunt, A.G., Bunch, T.E., Rampino, M., 2001. Impact event at the Permian–Triassic boundary: evidence from extraterrestrial noble gases in fullerenes. Science 291, 1530–1533.
Benton, M.J., Twitchett, R.J., 2003. How to kill (almost) all life: the end-Permian extinction event. Trends in Ecology & Evolution Vol.18 (No.7) July 2003.
Berner, R.A., 2002. Examination of hypotheses for the Permo–Triassic boundary extinction by carbon cycle modeling. Proceedings of National Academic Science of the United States of America 99, 4172–4177.
Berner, R.A., Kothavala, Z., 2001. GEOCARB III: a revised model of atmospheric CO2 over Phanerozoic time. American Journal of Science 301, 182–204.
Brandes, J.A., Devol, A.H., 2002. A global marine-fixed nitrogen isotopic budget: Implications for Holocene nitrogen cycling. Global Biogeochemical Cycles 16, 1120.
Brasier, M.D., 1995. Fossil indicators of nutrient levels, 1. Eutrophication and climate change. Geological Society of London. Special Publications 83, 113–132.
Brookfield, M.E., Twitchett, R.J., Goodings, C., 2003. Palaeoenvironments of the Permian Triassic transition sections in Kashmir. India: Palaeogeography, Palaeoclimatology, Palaeoecology 198, 353–371.
Erwin, D.H., Bowring, S.A., Jin, Y.G., 2002. End-Permian mass extinctions: a review. Boulder Geological Society of America Special Paper 356, 363–384.
Gibson, D.W., 1969. Triassic stratigraphy of the Bow River-Crowsnest Pass region, Rocky Mountains of Alberta and British Columbia. Geological Survey of Canada Paper 68 (29), 48.
Gibson, D.W., 1974. Triassic rocks of the Southern Canadian Rocky Mountains. Geological Survey of Canada, Bulletin 230, 65.
Gibson, D.W., Barclay, J.E., 1989. Middle Absaroka Sequence, The Triassic Stable Craton. In: Ricketts, B. (Ed.), Basin Analysis - The Western Canada Sedimentary Basin: Canadian Society of Petroleum Geologists Special Publication, pp. 219–231.
Grasby, S.E., Beauchamp, B., 2009. Latest Permian to Early Triassic basin-to-shelf anoxia in the Sverdrup Basin, Arctic Canada. Chemical Geology 264, 232–246.
Grice, K., Cao, C., Love, G.D., Bottcher, M.E., Twitchett, R.J., Grosjean, E., Summons, R.E., Turgeon, S.C., Dunning, W., Jin, Y., 2005. Photic zone euxinia during the Permian–Triassic superanoxic event. Science 307, 706–709.
Hays, L.E., Beatty, T., Henderson, C.M., Love, G.D., Summons, R.E., 2007. Evidence for photic zone euxinia through the end-Permian mass extinction in the Panthalassic Ocean. Paleoworld 16, 39–50 (Peace River Basin, Western Canada).
Henderson, C.M., 1989. Absaroka Sequence - The Lower Absaroka Sequence: Upper Carboniferous and Permian (Chapter 10) In: Ricketts, B. (Ed.), Basin Analysis - The Western Canada Sedimentary Basin: Canadian Society of Petroleum Geologists Special Publication, pp. 203–217.
Henderson, C.M., 1997. Uppermost Permian conodonts and the Permian–Triassic boundary in the Western Canada Sedimentary Basin. Bulletin of Canadian Petroleum Geology 45, 693–707.
Henderson, C.M., Richards, B.C., Barclay, J.E., 1994. Permian. In Mossop, G.D. (ed.) Geological Atlas of the Western Canada Sedimentary Basin Joint publication of the Canadian Society of Petroleum Geologists and the Alberta Research Council, pp. 251–258.
Hotinski, R.M., Bice, K.L., Kump, L.R., Najjar, R.G., Arthur, M.A., 2001. Ocean stagnation and end-Permian anoxia. Geology 29, 7–10.
Huey, R.B., Ward, P.D., 2005. Hypoxia, global warming, and terrestrial Late Permian extinctions. Science 308, 398–401.
Isozaki, Y., 1994. Superanoxia across the Permo–Triassic boundary: record in accreted deep-sea pelagic chert in Japan. In: Embry, A.F., Beauchamp, B., Glass, D.J. (Eds.), Pangea: Global Environments and Resources: Canadian Society of Petroleum Geologists, Memoir, vol. 17, pp. 805–812.
Isozaki, Y., 1997. Permo–Triassic boundary superanoxia and stratified superocean: records from lost deep-sea. Science 276, 235–238.
Isozaki, Y., 2009. Integrated “plume winter” scenario for the double-phased extinction during the Paleozoic–Mesozoic transition: The G-LB and P-TB events from a Panthalassan perspective. Journal of East Asian Earth Sciences 36, 459–480.
Jin, Y.G., Wang, Y., Wang, W., Shang, Q.H., Cao, C.Q., Erwin, D.H., 2000. Pattern of marine mass extinction near the Permian Triassic boundary in South China. Science 289, 432–436.
Kashiyama, Y., Ogawa, N.O., Kuroda, J., Shiro, M., Nomoto, S., Tada, R., Kitazato, H., Ohkouchi, N., 2008. Diazotrophic cyanobacteria as the major photoautotrophs during mid-Cretaceous oceanic anoxic events: nitrogen and carbon isotopic evidence from sedimentary porphyrin. Organic Geochemistry 39, 532–549.
Kidder, D.L., Worsley, T.R., 2003. Late Permian warming, the rapid latest Permian transgression, and the Permo-Triassic extinction. 2003 GSA Annual Meeting: Seattle, WA. .
Kidder, D.L., Worsley, T.R., 2004. Causes and consequences of extreme Permo– Triassic warming to globally equable climate and relation to the Permo–Triassic extinction and recovery. Palaeogeography, Palaeoclimatology, Palaeoecology 203, 207–237.
Kiehl, J.T., Shields, C.A., 2005. Climate simulation of the latest Permian: implications for mass extinction. Geology 33, 757–760.
Knoll, A.H., Bambach, R.K., Canfield, D.E., Grotzinger, J.P., 1996. Comparative Earth history and late permian mass extinction. Science, New Series 273 (5274), 452–457.
Korte, C., Kozur, H.W., 2010. Carbon-isotope stratigraphy across the Permian–Triassic boundary: a review. Journal of Asian Earth Sciences 39, 215–235.
Korte, C., Pande, P., Kalia, P., Kozur, H.W., Joachimski, M., Oberhänsli, H., 2010. Massive volcanism at the Permian–Triassic boundary and its impact on the isotopic composition of the ocean and atmosphere. Journal of Asian Earth Sciences 37, 293–311.
Kump, L.R., Pavlov, A., Arthur, M.A., 2005. Massive release of hydrogen sulfide to the surface ocean and atmosphere during interval of oceanic anoxia. Geology 33, 397–400.
Luo, G., Wang, Y., Yang, H., Algeo, T.J., Kump, L.R., Huang, J., Xie, S., 2011. Stepwise and large-magnitude negative shift in δ13Ccarb preceded the main marine mass extinction of the Permian–Triassic crisis interval. Palaeogeography, Palaeoclimatology, Palaeoecology 299, 70–82.
Mei, S., 1996. Restudy of conodonts from the Permian-Triassic boundary beds at Selong and Meishan and the natural Permian-Triassic boundary. In: Wang, H., Wang, X. (Eds.), Memorial Volume of Prof. Sun Yunzhu: Palaeontology and Stratigraphy. Centennial China University of Geosciences Press, Wuhan, pp. 141–148.
Mei, S., Henderson, C.M., 2001. Evolution of Permian conodont provincialism and its significance in global correlation and paleoclimatic implication. Palaeogeography, Palaeoclimatology, Palaeoecology 170, 237–260.
Meyer, K.M., Kump, L.R., 2008. Oceanic euxinia in Earth history: causes and consequences. Annual Review of Earth and Planetary Sciences 36, 251–288.
O'Leary, M.H., 1988. Carbon isotopes in photosynthesis. Bioscience 38, 328–336.
O'Leary, M.H., 1981. Carbon isotope fractionation in plants. Phytochemistry 20, 553–567.
Payne, J.L., Lehrmann, D.J., Wei, J., Orchard, M.J., Schrag, D.P., Knoll, A.H., 2004. Large perturbations of the carbon cycle during recovery from the end-Permian extinction. Science 305, 506–509.
Peter, D., Ward, P.D., Botha, J., De Kock, M.O., Erwin, D.H., Garrison, G., Kirschvink, J., Smith, R., 2005. Abrupt and Gradual Extinction Among Late Permian Land Vertebrates in the Karoo Basin, South Africa. www.sciencexpress.org/20January2005/Page1/10.1126/science.1107068 2005.
Raup, D.M., Sepokoski, J.J., 1982. Mass extinction in the marine fossil record. Science 215, 1501–1503.
Retallack, G.J., Smith, R.M.H., Ward, P.D., 2003. Vertebrate extinction across the Permian–Triassic boundary in Karoo Basin, South Africa. Geological Society of America Bulletin 115, 1133–1152.
Richards, B.C., 1989. Upper Kaskaskia Sequence: Uppermost Devonian and Lower Carboniferous. In: Ricketts, B. (Ed.), Basin Analysis - The Western Canada Sedimentary Basin: Canadian Society of Petroleum Geologists Special Publication, pp. 165–201.
Shen, S., Cao, C., Henderson, C.M., Wang, X., Shi, G.R., Wang, Y., Wang, W., 2006. End-Permian mass extinction pattern in the northern peri-Gondwanan region. Palaeoworld 15, 3–30.
Shen, S.Z., Henderson, C.M., Bowring, S.A., Cao, C.Q., Wang, Y., Wang, W., Zhang, H., Zhang, Y.C., Mu, L., 2010. High-resolution Lopingian (Late Permian) timescale of South China. Geological Journal 45, 122–134.
Sigman, D.M., Boyle, E.A., 2000. Glacial/interglacial variations in atmospheric carbon dioxide. Nature 407, 859–869.
Taylor, E.T., Taylor, T.N., Cúeno, R., 2000. Permian and Triassic high latitude paleoclimates: evidence from fossil biotas. In: Huber, B., Macleod, K., S.W. (Eds.), Warm Climates in Earth History: Cambridge. Cambridge University Press, pp. 321–350.
Tribovillard, N., Algeo, T.J., Lyons, T., Riboulleau, A., 2006. Trace metals as paleoredox and paleoproductivity proxies: an update. Chemical Geology 232, 12–32.
Ward, P.D., Montgomery, D.R., Smith, R., 2000. Altered river morphology in South Africa related to the Permian–Triassic extinction. Science 289, 1740–1743.
White, R.V., 2002. Earth's biggest ‘whodunnit’: unravelling the clues in the case of the end-Permian mass extinction. Philosophical Transactions of the Royal Society of London, Series B 360, 2963–2985.
Wignall, P.B., Hallam, A., 1992. Anoxia as a cause of the Permian/Triassic mass extinction: facies evidence from northern Italy and the western United States. Palaeogeography, Palaeoclimatology, Palaeoecology 93, 21–46.
Wignall, P.B., Hallam, A., 1993. Griesbachian (Earliest Triassic) palaeoenvironmental changes in the Salt Range, Pakistan and southeast China and their bearing on the Permo-Triassic mass extinction. Palaeogeography, Palaeoclimatology, Palaeoecology 102, 215–237.
Wignall, P.B., Newton, R., 2003. Contrasting deep-water records from the Upper Permian and Lower Triassic of South Tibet and British Columbia: evidence for a diachronous mass extinction. PALAIOS 18, 153–167.
Wignall, P.B., Twitchett, R.J., 1996. Oceanic anoxia and the end Permian mass extinction. Science 272, 1155–1158.
Winguth, A.M.E., Heinze, C., Kutzbach, J.E., Maier-Reimer, E., Mikolajewicz, U., Rowley, D., Rees, A., Ziegler, A.M., 2002. Simulated warm polar currents during the middle Permian. Paleoceanography 17 (4), 1057. doi:10.1029/2001PA000646.